



LANDSCAPE IMAGE DEFOGGING SYSTEM BASED ON DCP ALGORITHM OPTIMIZATION

KUNJIA SUN* AND JIANWEI GUO†

Abstract. As the global climate environment deteriorates gradually, the collected images are covered by fog, which reduces the clarity of the images. Therefore, the processing of fog images is very important. In landscape image defogging research, the defogging process may be affected by factors such as data quality, noise interference, and computational efficiency. To improve the defogging effect of landscape fog images, a landscape image defogging system was put forward with the optimization of dark channel prior algorithm. The image defogging algorithm was combined with the improved atmospheric scattering model estimation algorithm and the dark channel convolutional network image defogging algorithm to achieve image defogging. The atmospheric light estimation method based on atmospheric scattering model combined transmittance map and grayscale map information to achieve optimization of defogging effect. In the improvement of the dark channel prior algorithm, a convolutional network was introduced for feature extraction to enhance the smoothing of image brightness changes and transmittance estimation. The research findings demonstrated that the signal-to-noise ratio of the image defogging algorithm estimated by the atmospheric scattering model could reach up to 19dB, which was about 15.4% higher than that of existing 5 image defogging algorithms on average, indicating that the image resolution of the algorithm was higher after defogging. In the Reside dataset, the image defogging algorithm based on dark channel prior increased the signal-to-noise ratio by about 9.5%, the average gradient by about 10.4%, the structural similarity by about 12%, and the information entropy by about 5.8%, indicating that the effect of the algorithm was stable and the image defogging effect was good. The dark channel convolutional network image defogging algorithm had less running time and reduced the complexity of the defogging structure, by contrast, it reduced the running time by about 67%. The average scores for the operability, stability, and defogging effect of the system were 9.87 points, 9.85 points, and 9.54 points, respectively, indicating good performance of the system. The user feedback on natural landscape fog maps, architectural landscape fog maps, and historical landscape fog maps is good, and the user experience is high.

Key words: Image defogging; Atmospheric scattering model; Dark channel prior; Landscape image; Signal-to-noise ratio

1. Introduction. Humans intuitively feel the world through vision, and visual images carry a lot of information about objects [1]. According to statistics, 75% of human information comes from visual images. Image is a way of information transmission, which contains a variety of information. The compressed space is smaller, which is benefit to improve the propagation speed, and the propagation distance can be further explored [2]. As the speed growth of science and technology and the improvement of human living standards, cameras, mobile phones and other devices can obtain images through the camera function. Image technology is widely used in traffic navigation, tourism guide and other fields, which helps human to obtain useful information and further improve work efficiency [3]. In image acquisition, the camera equipment will encounter the impact of environmental factors such as fog and stratification, resulting in the reduction of the clarity of the image acquisition, which seriously affects the subsequent image processing work [4]. The development of modern industry leads to the aggravation of environmental pollution, and the most representative is the fog weather, which seriously affects human life and work, especially the traffic [5]. The image acquisition of the camera equipment includes target scene reflection imaging and natural or artificial light source projection imaging. In hazy weather, optical fiber scattering is serious, which reduces the clarity and contrast of imaging, leading to the loss of image information [11]. To improve the function of landscape image defogging (IDF), a system based on dark channel prior (DCP) algorithm was raised in this paper. IDF was completed by improving the DCP image processing technology to improve users' system experience. The research is divided into four parts. The first part is a summary of the research on the existing IDF algorithm. The second part is the research

*China Society of Labor Economics, Artificial Intelligence Professional Committee, Beijing, 100044, China

†Beijing Jiaotong University, School of Traffic and Transportation, Beijing, 100044, China (jianwei_guo123@outlook.com)

on the landscape IDF algorithm and the design of the landscape IDF system optimized based on the DCP algorithm. The third part is the effect verification of the landscape IDF algorithm and system optimized based on the DCP algorithm. The fourth part is the summary of the whole article.

2. Related Works. IDF enhances the contrast and color saturation of the image, thus making the image more vivid and stark. D. Fan's research team proposed a dark channel iterative defogging algorithm based on pixel-level atmospheric illumination map, built a relationship model combining fog density and depth of field, and realized the optimal control of defogging degree by iteration. It was proved that the algorithm could well solve the problem of sky oversaturation [7]. Zhao research group proposed an IDF algorithm design, which realized the quantization optimization of atmospheric illumination by using pixel average, and introduced the understanding edge order factor to find pixel position. The laboratory findings demonstrated that the algorithm could correct the effect of white area in the image [8]. Long et al. put forward an IDF algorithm based on field programmable gate array (FPGA), which used data transmission module to realize data interaction and combined with convolutional neural network (CNN) to realize IDF. The research results showed that the algorithm had good adaptive ability [9]. He research group proposed a comprehensive IDF network based on the improved atmospheric scattering (AS) model and the fusion of attention features, and combined with the five-layer convolutional network to achieve image restoration. The experiment outcomes expressed that this method could effectively defog and has good stability [10]. Sun group proposed a three-channel RGB unmanned aerial vehicle IDF method based on the non-local feature structure tensor, combined with the dark channel theory to build an IDF model, and used the image non-local tensor to protect the image edge information. The research findings denoted that this method could effectively avoid the halo effect [11]. The DCP defogging algorithm relied on the AS model for defogging processing. Through the observation and summary of massive images with fog and without fog, some existing mapping relationships were obtained. Rafid Hashim's team used color space and DCP to realize single fog image processing, and used adaptive histogram equalization to adjust contrast and brightness. The analysis outcomes demonstrated that the image quality value of this method was high [18]. Sun et al. proposed an improved real-time IDF algorithm based on DCP and fast weighted guided filtering. K-means algorithm was used to achieve clustering of bright and dark areas in images, and the transmission map was generated by combining fast weighted guided filtering algorithm. The research outcomes expressed that this method could effectively improve the color difference and retain more image details [13]. The research team of K. Ke proposed a single IDF algorithm based on the DCP principle. Combining the median and minimum filters could obtain the accurate acquisition of the dark channel value. And combined with the AS model could obtain the fog free image. The experimental findings illustrated that the algorithm could effectively improve the degradation of image quality [14]. Aiming at the sparsity of dark channel, the research group of X. Yu proposed an IDF method based on fractional DCP, which used fractional dark channel to realize kernel estimation of intermediate image, and used semi-quadratic splitting to solve non-convex problem. The laboratory findings indicated that this method had a good effect in synthesizing real image [15]. Kwak research team proposed the optical flow technology based on the Lucas-Kanade method to detect the area of smoke, and realized the image preprocessing by using the DCP, and combined with the CNN to determine the properties of the region. The outcomes denoted that the accuracy of the method was 4% higher than that of the object detection model without image preprocessing [16].

To sum up, many scholars and researchers have conducted a great deal of research and design for IDF and DCP algorithms, but the applicability of these models and algorithms still needs to be improved. Therefore, this paper proposed a landscape IDF system optimized based on DCP algorithm, hoping to improve the function of landscape IDF and enhance the user's visual experience.

3. Landscape IDF Algorithm. In this chapter, DCP theory and clustering segmentation quad fork number are used to promote the IDF algorithm, and the algorithm estimated by AS model is proposed. The initial transmission of AS is calculated with logarithmic transformation adaptive, and the transmission optimization is completed with L1 regularization.

3.1. IDF Algorithm Based on AS Model Estimation. At present, the environmental problems are relatively serious, such as the frequent occurrence of extreme weather such as fog and sand dust, so that the quality of outdoor landscape image acquisition is seriously reduced, which influences the effectiveness of

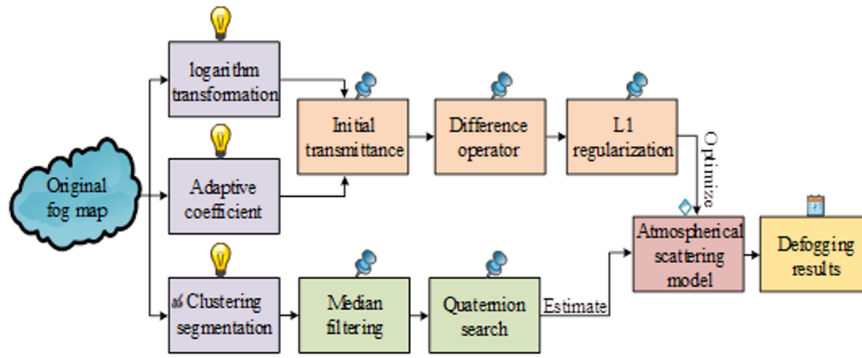


Fig. 3.1: The Principle of IDF Algorithm Based on AS Model Estimation

computer vision system. The degraded image restoration has become an important part of image processing [17]. Based on the AS model, the DCP uses the gray law of clear outdoor images to define the channel of low pixel gray points as the dark channel. When not considering the interference of brighter areas such as the sky, there is at least one color channel in the RGB three channels of each pixel's neighborhood that has a minimum brightness value approaching 0. These very low pixel grayscale are called dark pixels. The expression of the image dark channel is shown in equation 3.1.

$$J^{\text{dark}}(x) = \min_{y \in \Omega(x)} \left(\min_{c \in \{r, g, b\}} J^c(y) \right) \Rightarrow 0 \quad (3.1)$$

In equation 3.1, the dark channel of the image is denoted by $J^{\text{dark}}(x)$. The central neighborhood window of the pixel point $J^{\text{dark}}(x)$ is denoted by $\Omega(x)$. The pixel points in the neighborhood $\Omega(x)$ are indicated by y , and one of the RGB channels of the fog free image is expressed by $J^c(y)$. The existing DCP algorithm has limitations such as Halo effect in its defogging effect. Therefore, the research improves the DCP algorithm and proposes an IDF algorithm based on AS model estimation. The principle of the algorithm is shown in Figure 3.1. The transmittance estimation of DCP is insufficient. This study improves the estimation methods of transmittance and atmospheric light, and combines logarithmic transformation to improve the adaptive ability of transmittance to defog, so as to improve the distortion in the mutation region. The foggy image degradation model is shown in equation 3.2 after small channel processing.

$$t(x, y) = \frac{\min_{c \in \{r, g, b\}} A - \min_{c \in \{r, g, b\}} I^c(x, y)}{\min_{c \in \{r, g, b\}} A - \min_{c \in \{r, g, b\}} J^c(x, y)} \quad (3.2)$$

In equation 3.2, coordinates of fog image and non-fog image are represented by (x, y) . Their transmittance is expressed by $t(x, y)$. Gray values in the channel c are respectively denoted by $I^c(x, y)$ and $J^c(x, y)$, and atmospheric light at infinity is labeled by A . Equation 3.2 is simplified as shown in equation 3.3.

$$t(x, y) = \frac{A^c - I^{\text{dark}}(x, y)}{A^c - J^{\text{dark}}(x, y)} \quad (3.3)$$

In equation 3.3, it is assumed that atmospheric light is a constant and denoted by $A^c I^{\text{dark}}(x, y)$ and $J^{\text{dark}}(x, y)$ mean simplified forms of $\min_{c \in \{r, g, b\}} I^c(x, y)$ and $\min_{c \in \{r, g, b\}} J^c(x, y)$, respectively. The definition of existing single IDF algorithms suggests that there is a linear relationship between the minimum brightness of the channel for both fog free and non-fog free images, but the unknown parameters of the linear curve are difficult to solve [18]. In the complex terrain environment, with the change of the fog concentration, the pixel brightness of the fog image will also change, and the fog concentration at the shadow shelter is different, resulting in the uneven distribution of the fog image brightness [19]. Simple linear transformation cannot achieve the

estimation of image dark channel brightness, and its grayscale difference defense cannot be described, resulting in a large error in transmittance estimation and affecting the defogging effect. The brightness response observed by the naked eye is nonlinear. The study introduces the parameter k_d to represent the adjustable grayscale dynamic range and achieve smooth processing of brightness differences in dark channels. The linear method estimates the dark channel of the line due to the influence of fog, causing distortion during image restoration. The logarithmic change can reduce the intensity value, avoid the influence of high brightness areas, and achieve natural transition of the dark channel area image. After smoothing the edge information of the deep field area of the image, it is more suitable for estimating the dark channel of the scene brightness, which helps to improve the effectiveness of transmittance estimation. The initial transmittance expression under logarithmic variation is shown in equation 3.4.

$$t(x, y) = \frac{|A^c - \min_{c \in \{r, g, b\}} I^c(x, y)|}{|A^c - \log \left(\frac{(\min_{c \in \{r, g, b\}} I^c(x, y)) - RGB_{\min}}{RGB_{\max} - RGB_{\min} (\min_{c \in \{r, g, b\}} I^c(x, y)) + k_d} \right)|} \quad (3.4)$$

In equation 3.4, the minimum and maximum values of $\min_{c \in \{r, g, b\}} I^c(x, y)$ are respectively expressed by RGB_{\min} and RGB_{\max} . The lack of available scene structure information in a single image increases the difficulty of defogging a single image. There is a linear relationship among fog concentration, depth of field, brightness and saturation. The prior law of fog image color decay is shown in equation 3.5.

$$d(x) \propto c(x) \propto v(x) - s(x) \quad (3.5)$$

In equation 3.5, depth of field is denoted by $d(x)$. Fog concentration is represented by $c(x)$, and the difference between brightness and saturation of the image in the color model of hexagonal vertebra is expressed by $v(x) - s(x)$. The scene saturation and brightness of clear close-range and misty areas are moderate, and the difference between the two is small. When the fog gradually increases, the brightness rises with the decrease of saturation, leading to the difference between the two becomes larger, and it is difficult to distinguish the color in the scene. Compensation of transmittance in the sky area is shown in equation 3.6.

$$t_b(x, y) = \max(\phi |V - S|, t(x, y)) \quad (3.6)$$

In equation 3.6, the difference adjustment factor of brightness and saturation is represented by ϕ , and the sky transmittance is represented by $t_b(x, y)$. At this time, the difference between brightness and saturation of the image is indicated by $|V - S|$. When the difference adjustment factor of brightness and saturation is large, the transmittance deviation is large, and the effective compensation of transmittance can be realized if the value is small. The regularization expression of the weighted L1 norm is shown in equation 3.7.

$$Q(x, y) = \{t_b(x) - t_b(y)\} \quad (3.7)$$

In equation 3.7, adjacent pixels in the transmittance figure are represented by x and y , and the weighting function is represented by $Q(x, y)$, to complete the adjustment of transmittance difference. The transmittance difference depth information between pixels changes with the depth of the scene, and the more obvious the reflection of the weighting function is. The weighting function needs to reflect the depth difference information, and it is very difficult to directly use the depth map to construct the weighting function. The research uses the square variance of gray values of two adjacent pixels to construct the weighting function, as shown in equation 3.8.

$$Q(x, y) = e^{-\frac{\|I(x) - I(y)\|^2}{2\delta^2}} \quad (3.8)$$

In equation 3.8, the standard deviation is represented by δ , and the difference of gray values between adjacent pixel points is expressed by $I(x) - I(y)$. Image edge gradient jump changes can be described by detection operators, and more details can be provided. In this study, a filter kernel high-order difference operator is introduced to realize discrete convolution. The high-order difference operator is shown in Figure 3.2.

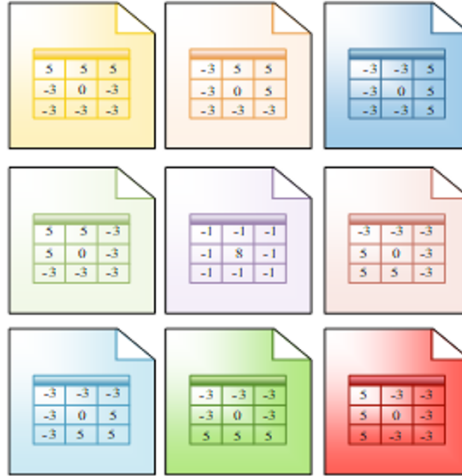


Fig. 3.2: High-order Difference Operator

The number of higher-order difference operators used in this study is 9. Discrete convolution is carried out in equation (8), and then the simplified expression is shown in equation 3.9.

$$\sum_{j \in \eta} \|Q_j \star (D_j \otimes t)\|_1 \quad (3.9)$$

In equation 3.9, the index set of the original fog image region is represented by η . The convolution operation is represented by \otimes . The set of higher-order difference operators is represented by D_j . Color attenuation priors focus on defogging effect and ignore problems such as color bias and edge blurring. The introduction of L1 norm can improve the fidelity of compensation transmittance of color attenuation priors. The minimization expression of L1 norm is shown in equation 3.10.

$$\theta \|t_b - t_z\|_2^2 + \sum_{j \in \eta} \|Q_j \star (D_j \otimes t_b)\|_1 \quad (3.10)$$

In equation 3.10, the regularization parameter is represented by θ . The transmittance after iteration is represented by t_z . The transmittance after compensation is represented by t_b . Since the DCP algorithm has atmospheric failure, the paper improves the algorithm by combining with clustering segmentation quadrangle number. Cluster analysis is an unsupervised learning method, which is broadly utilized in various engineering fields of data mining and statistics. In IDF, K-means is commonly used to cluster the Euclidean distance and complete the estimation of the transmission of the sky region [20]. The single clustering of RGB three-channel will lead to the inconsistency of gray color channels of pixels. The three-channel pixels are converted into single-channel gray maps, as shown in equation 3.11.

$$G(i, j) = \text{avg}_{c \in \{r, g, b\}} I^c(x) \quad (3.11)$$

In equation 3.11, the gray value of fog image is denoted by I , and the gray value of location (i, j) in a two-dimensional plane is denoted by $G(i, j)$. The clustering method is applied in image segmentation to improve the accurate calculation of atmospheric light.

3.2. IDF Algorithm Optimization and System Design Based on DCP. The DCP mechanism is constrained by various conditions, and its value is also affected. In this paper, a dark channel IDF algorithm is proposed by combining the feature pixel extraction idea of dark channel and convolutional network. The way

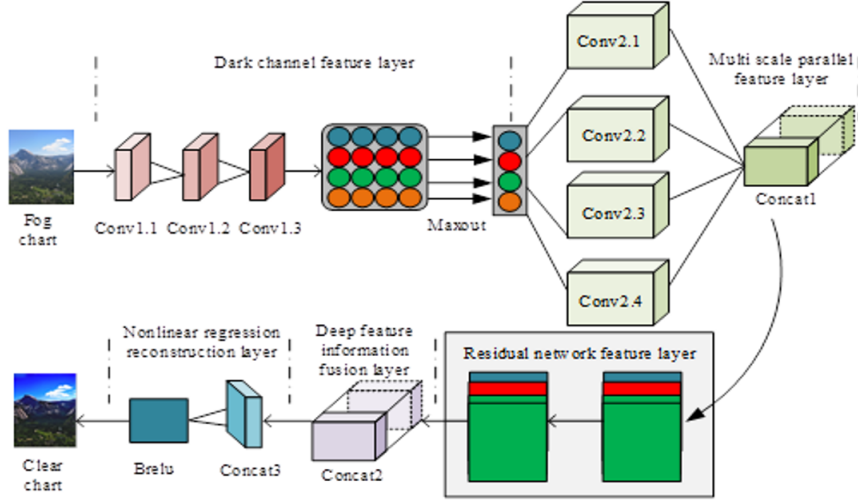


Fig. 3.3: The Overall Structure of DCNN Defogging Algorithm

of network independent feature extraction can solve the limitations of DCP algorithm, and help to improve the clarity of defogging [21, 22]. The training and test sets of the model utilize Reside data set. Then, feature extraction is carried out using the dark channel idea. The IDF model of the dark channel convolutional network (DCNN) is built through convolution components, etc. Parameter debugging is used to optimize the model, and the final model is used to complete the fog image processing. The overall structure of the DCNN defogging algorithm is displayed in Figure 3.3.

Dark channel feature layer is used to realize feature crude extraction and activated under Maxout function. The network input is the standard fog map with the size of 480×640 . The output depth of the first two layers is 16. The filter window size is 5×5 . the step size is 1 unit. The original input image is pre-extracted and mapped through the convolution kernel, and then the high-dimensional feature map is obtained. The filtering window size of the last layer is 3×3 . The step size is one unit. The depth of the convolution kernel is 16. The DCP filtering is completed under the activation of Maxout function. The function of Maxout function is to group and map the convolution feature graph to obtain the key feature information of the fog graph V [23, 24]. The operation of Maxout function is shown in equation 3.12.

$$F_1^j = \max_{i \in [1, 16], j \in [1, 4]} \{ \text{conv}(W_1^{(i,j)} \times I + B_1^{(i,j)}) \} \quad (3.12)$$

In equation 3.12, the input fog map is represented by I . The amount of convolutional feature maps at the output end of the first three layers is denoted by i . The amount of output feature maps is represented by j . The filtering weight and bias of each feature map are denoted by W_i and B_i respectively. The convolution operation is expressed by conv . The output of the dark channel feature layer is indicated by F_1 . In this study, four groups of convolution kernels with different sizes are used to extract deep feature information in parallel. Multi-scale convolution operation is shown in equation 3.13.

$$F_i = W_i \times F_1 + B_i \quad (i \in \{2, 3, 4, 5\}) \quad (3.13)$$

In equation 3.13, the weights and bias of different convolution kernels are expressed by W_i and B_i , respectively. The output of the i th layer is expressed by F_i . Different feature maps are combined by parallel layers to obtain a feature map with a size of $32 \times 480 \times 640$, which increases the number of feature maps. The convolution operation of each feature layer is shown in Figure 3.4.

Figure 3.4(a) shows the parallel operation of the multi-scale parallel convolutional layer. After extracting different features, the feature graph structure and information will be lost. In this study, the improved cavity

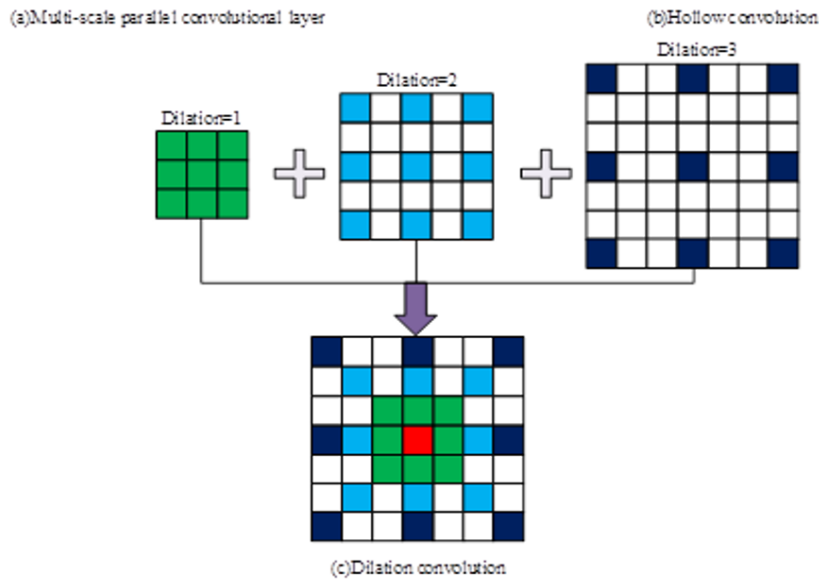


Fig. 3.4: Convolutional Operation of Each Feature Layer

convolution is utilized to the residual network to realize the detailed extraction of feature information. With the increase of the empty weight interval between the ordinary convolution and the sum, void convolution is formed, as shown in Figure 3.4(b). When the size of the convolution kernel of the filter window is 3×3 and the number of weight intervals is 1, the expansion rate is 2. The range perception is the same as that of the filter kernel of the filter window size 5×5 , but the calculation is more convenient and fast. The training effect of the convolutional network does not increase with the increase of the depth of the network layer. When the number of layers of the network structure increases to a certain number, the training effect may become worse, causing network degradation. The residuals unit realizes the layered learning of the residuals between input and output through channel association. Hollow convolution can extend the range of visual field and increase the spatial hierarchy of features, but the weight of hollow convolution is discontinuous, resulting in the perceived visual field cannot contain all image features. Grid halo will occur in subsequent fusion, which will reduce the IDF effect. In this study, expansive convolution is applied to feature extraction of residuary units of different sizes. The principle of expansive convolution is shown in Figure 3.4(c). The inner convolution kernel is used to achieve the coherence of image feature information, and the structure hierarchy of feature space is completed through the outer convolution kernel, which reduces the degree of gradient dispersion and contributes to the propagation of detailed feature information. The number of units in the feature layer of the residual network is 6, and the components of each unit include the convolution module, batch normalization and activation functions. The amount of convolution cores of the first three residuals blocks is 4, the size is $4 \times 3 \times 3$, and the size of the output feature graph is $4 \times 480 \times 640$. The latter three residuals contain 12 convolutional blocks respectively, and the output feature graph size is $12 \times 480 \times 640$, with a residual convolution step size of 1 unit.

The output features of convolutional layer of CNN include three indexes: channel number, graph height and width. Increasing the amount of network layers will reduce the feature extraction effect and affect the IDF effect and the integrity of feature information. In the depth feature information fusion layer, the height and width of the feature map are fixed, and the feature map of the convolutional kernel is splice by means of channel dimension extension. The fusion rule is shown in equation 3.14.

$$(c, h, w) \rightarrow (\alpha \cdot c, h, w) \quad (3.14)$$

In equation 3.14, the number of channels is represented by equation. The height of the feature graph is denoted by h . the width of the feature graph is indicated by w . And the number of the increased feature graph

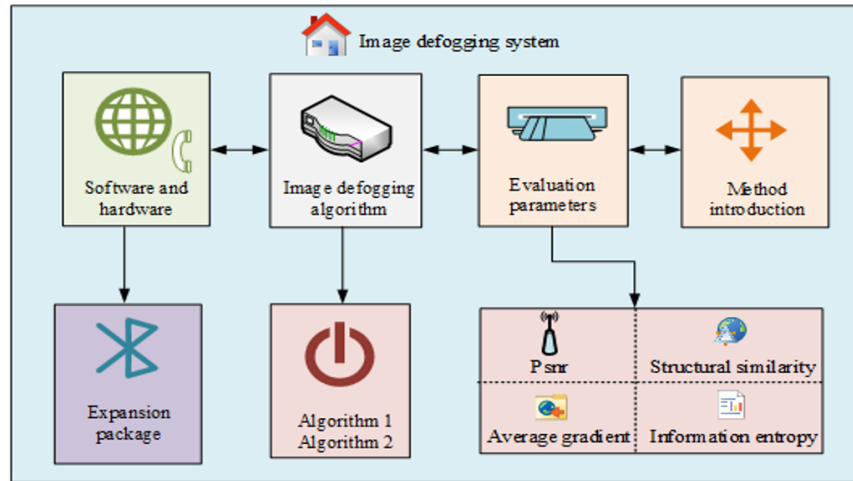


Fig. 3.5: Design Block Diagram of Landscape IDF System Optimized Based on DCP Algorithm

is represented by α . The depth feature information fusion layer realizes the refinement of the feature map, and obtains the feature map with the size of $48 \times 480 \times 640$, which increases the amount of output feature maps and helps to transfer rich and effective details of the feature information. The nonlinear regression reconstruction layer is composed of independent convolution layers to realize the mapping between feature space and image space. The effect of network prediction is measured by the target loss function L_{MSE} , which is shown in equation 3.15.

$$L_{MSE} = \frac{\sum_{i=1}^N \|F_{10}^i - I^i\|_2^2}{NUM} \quad (3.15)$$

In equation 3.15, the clear image of group i and the predicted output image are expressed by I^i and F_{10}^i , respectively, and the number of sample training is labeled by NUM . The research constructs a defogging system through the above algorithms. The design block diagram of landscape IDF system optimized based on DCP algorithm is shown in Figure 3.5.

The basis of the system software design is the extension pack in the VS code editor, and the defogging system contains four functional areas. The first functional area is the system introduction and use area. Through the explanation of operation methods, points of attention and so on, the user's convenient use can be achieved. The second functional area is the objective performance evaluation area of the image, which mainly displays the parameters such as peak signal-to-noise ratio (SNR) and information entropy of the defogging algorithm to realize the evaluation of the defogging image. The third functional area is the selection area of IDF function, including two improved defogging algorithms, which can realize IDF and save the results through algorithm loading and use. The fourth functional area is the proposed system area, through which the system exits the system after IDF and saving [25, 26].

4. Effect Verification of Landscape IDF System Optimized Based on DCP Algorithm. This chapter is to evaluate the effect of the algorithm and model proposed in the second chapter. The first section of this chapter is to verify the effect of IDF algorithm estimated by the AS model. The second section is to verify the effect of IDF algorithm based on DCP. The third section is to verify the effect of landscape IDF system optimized based on DCP algorithm [27, 28, 29].

4.1. Effect Verification of IDF Algorithm Estimated by AS Model. To verify the effect of the IDF algorithm estimated by the AS model proposed in this study (algorithm Dq for short), He, Meng, Tarel, Berman and Lin algorithms were compared in the experiment. The He algorithm is an AS model estimation

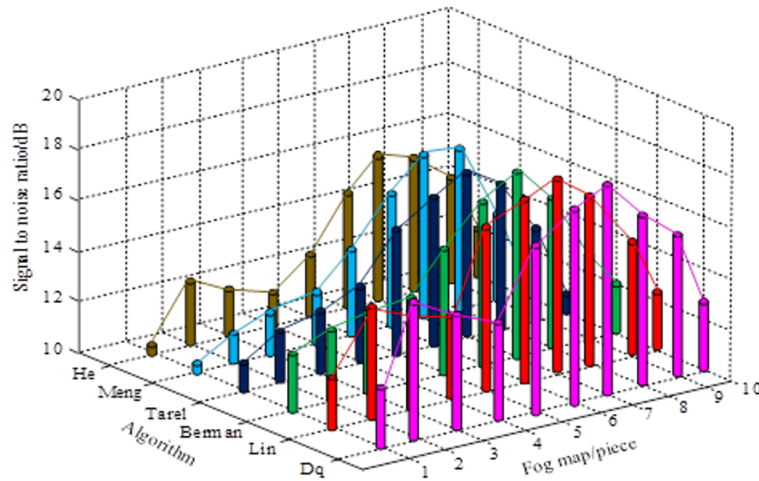


Fig. 4.1: SNR of Each Algorithm

algorithm based on scattering models proposed in 2020. It uses a set of filters applied to the observed image, multiplies the scattering terms in the image with the filters, and uses the backprojection method to invert the estimated values into an AS model. Meng algorithm is a deep learning-based AS model estimation algorithm proposed by Meng et al. in 2022. It uses CNN to encode images and uses backpropagation algorithms to invert the estimated values into AS models. The Tarel algorithm is an AS model estimation algorithm based on image segmentation proposed by Tarel in 2020. The Berman algorithm is a statistical model-based AS model estimation algorithm proposed in 2020. The Lin algorithm is an AS model estimation algorithm based on the least squares method proposed in 2022. It uses the least squares method to fit the observed images and predicts the AS model using a scattering model. In this experiment, a light source and a receiver (such as a camera or eye) will be used to verify the effect of different AS models on image defogging. The experiment will be conducted in an atmospheric environment with high relative humidity to simulate foggy conditions. It set parameters for the AS model, including simulating particle concentration, particle size, scattering angle, and speed of light for different foggy days. The particle concentration was 1010 particles per cubic centimeter, the particle size was 0.1 micrometers, the scattering angle was 30 degrees, and the speed of light was 3×10^8 meters per second. The SNR of each algorithm is shown in Figure 4.1.

In Figure 4.1, the highest SNR of He, Meng, Tarel, Berman and Lin algorithms was 15.1dB, 16.2dB, 16.3dB, 17.3dB and 17.4dB, respectively. The SNR of the IDF algorithm estimated by the AS model was the highest, up to 19dB, which was an average improvement of about 15.4% in contrast to the other five algorithms, indicating that the image of the algorithm after defogging was clearer and retained more useful feature information. The average gradient of the defogging effect of each algorithm is shown in Figure 4.2.

In Figure 4.2, the average gradient of the IDF algorithm estimated by the AS model was the highest, up to 14.2, which was about 11.37% higher than the other five algorithms on average, indicating that the image under this algorithm was not easy to distort and was conducive to visual experience. The structural similarity and information entropy results of the defogging effect of each algorithm are shown in Figure 4.3.

Figure 4.3a expresses the structural similarity results of defogging effects of various algorithms. The structural similarity index of IDF algorithm estimated by the AS model proposed in this study was relatively high, which was about 9.3% higher than other algorithms on average, and the fluctuation was not very obvious, indicating that the IDF algorithm could retain more detailed structural information. Figure 4.3b shows the information entropy result of the defogging effect of each algorithm. The information entropy index of the IDF algorithm estimated by the AS model proposed in this study was the highest, which increased by about 3% on average, indicating that the image of this algorithm was the most authentic after defogging. A comprehensive

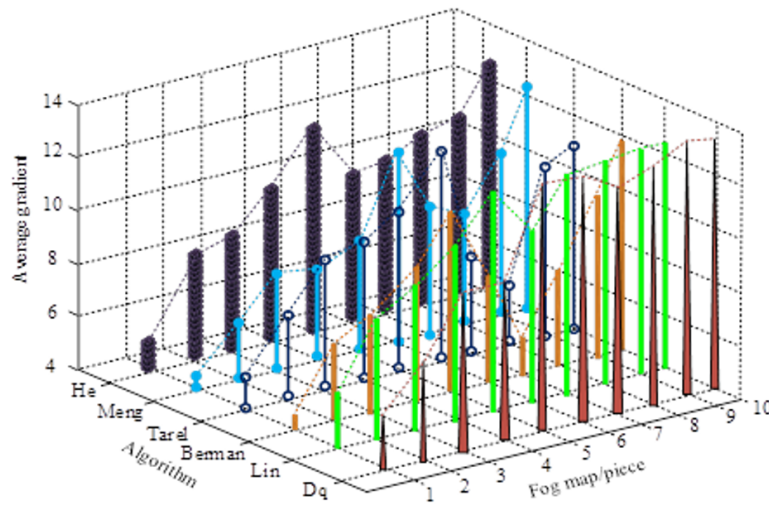
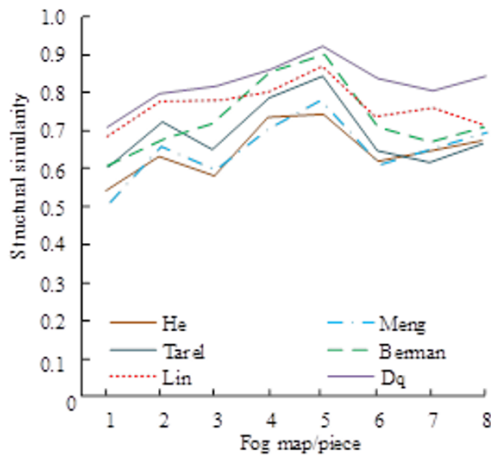
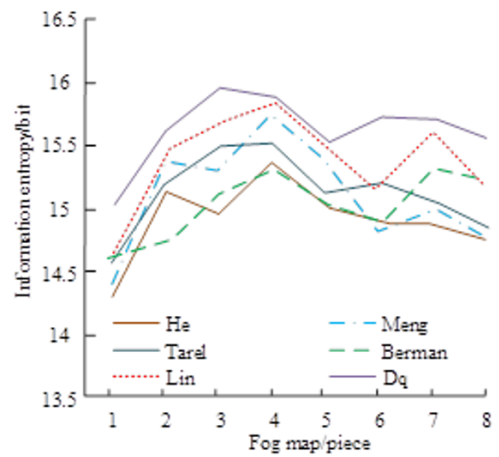


Fig. 4.2: The Average Gradient of the Defogging Effect of Each Algorithm



(a) Structural Similarity



(b) Information Entropy

Fig. 4.3: Structural Similarity Results of Defogging Effects of Various Algorithms

analysis showed that the IDF algorithm estimated by the AS model had a good defogging effect, which met the requirements of algorithm improvement.

4.2. Verification of IDF Algorithm Effect Based on DCP. The data set of the DCP-based IDF algorithm was Reside that contained abundant indoor and outdoor fog images. The composition of Reside date set is shown in Table 4.1.

Reside data set consisted of five sub-datasets, each of which had different functions and purposes. Indoor and outdoor data sets resided in training to achieve a simple and quick training process. Integrated target and mixed subjective test sets resided in testing and detection. The training results of the DCNN IDF algorithm are shown in Figure 4.4.

In Figure 4.4, the experiment adopted Gaussian distribution with mean of 0 and variance of 0.002 to realize

Table 4.1: Reside Data Set Composition

Type	Explain	Classification 1	Classification 2	Classification 3	Classification 4
ITS	Indoor training devices and equipment.	30000	40000	25000	15000
OTS	Outdoor training devices and equipment.	72000	65000	88000	98950
SOTS	Comprehensive test set for the target.	260	230	270	240
RTTS	A test set driven by real scenarios.	1332	2256	1123	1867
HSTS	Subjective mixed test set.	5	3	8	4

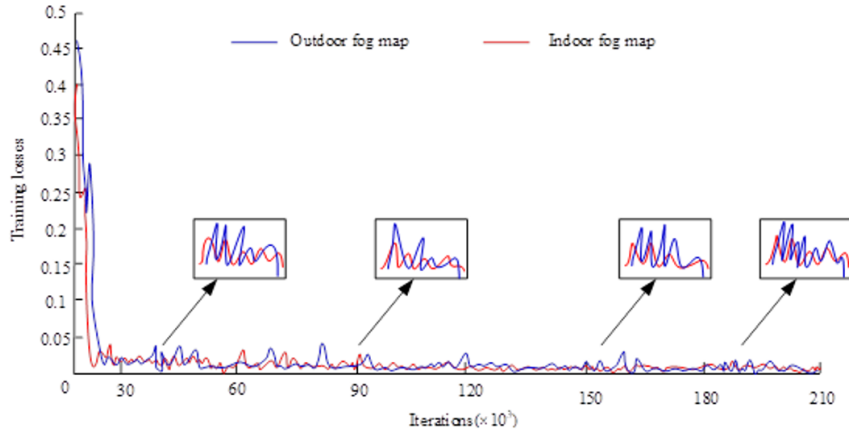


Fig. 4.4: The Training Results of the DCNN IDF Algorithm

weight initialization, and combined gradient descent algorithm for training. The loss reduction speed was fast in the first 30×10^3 training. When the number of iterations increased, the change of depth of field in outdoor scenes was more obvious, which was conducive to the improvement of defogging effect in real scenes. To verify the effect of IDF algorithm based on DCP, He, Cai, Ren and Li algorithms were compared in the experiment. The defogging effect data of each algorithm on 4 groups of indoor images are displayed in Table 4.2.

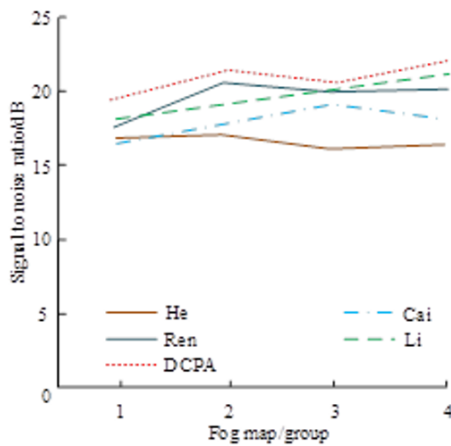
From Table 4.2, the SNR, average gradient, structural similarity and information entropy indexes of the IDF algorithm based on DCP were all higher than those of other algorithms. Among the defogging effects of the four groups of images, the SNR of the IDF algorithm based on DCP was above 20, the structural similarity was above 0.9, and the information entropy was above 15. It showed that the IDF algorithm based on DCP had better performance, and the IDF had smaller distortion and was clearer. Figure 4.5 shows the defogging effect data of 2 groups of outdoor images applied by each algorithm.

Figure 4.5a shows the defogging effect data of the first group of outdoor fog images. The algorithm based on DCP had the highest structural similarity and higher SNR and information entropy. Figure 4.5b shows the defogging effect data of the second group of outdoor fog images. Each index of the IDF with DCP was the highest, which meant it had better defogging effect, could retain more image details, and had stronger authenticity after defogging. The defogging effect data of each algorithm on 4 groups of real landscape fog images are shown in Figure 4.6.

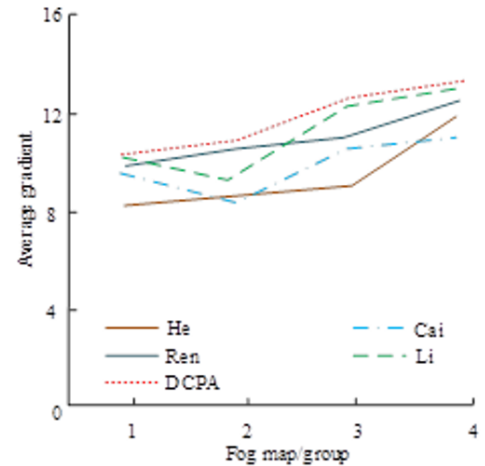
In Figure 4.6, all indexes of the proposed DCP-based IDF algorithm were higher than those of the other four algorithms, among which the indexes of Ren and Li algorithms were not much different from those of the DCP-based IDF algorithm. However, the defogging effect of these two algorithms on complex images was unstable and poor. The analysis of experimental data showed that, by contrast, the IDF algorithm based on

Table 4.2: The Defogging Effect Data of Each Algorithm on Four Sets of Indoor Images

Indoor fog map	Objective indicators	He	Cai	Ren	Li	DCP
Set 1	SNR/dB	15.61	15.22	16.41	18.12	20.22
	Average gradient	9.42	8.41	9.73	9.61	10.61
	Structural similarity	0.76	0.84	0.86	0.88	0.92
	Information entropy/bit	15.02	15.14	15.53	15.08	16.38
Set 2	SNR/dB	15.58	18.23	17.97	18.25	21.65
	Average gradient	8.82	9.41	10.42	9.87	10.87
	Structural similarity	0.78	0.79	0.82	0.85	0.91
	Information entropy/bit	15.14	16.23	15.23	16.21	17.56
Set 3	SNR/dB	18.01	20.11	19.09	20.42	23.56
	Average gradient	8.82	9.52	11.02	10.61	11.54
	Structural similarity	0.83	0.82	0.88	0.86	0.92
	Information entropy/bit	13.25	14.26	14.52	15.29	16.23
Set 4	SNR/dB	17.23	18.25	20.01	20.78	22.98
	Average gradient	8.08	7.51	8.99	8.25	9.62
	Structural similarity	0.71	0.77	0.84	0.81	0.91
	Information entropy/bit	14.92	13.58	14.18	13.94	15.35



(a) The first set of fog maps



(b) The second set of fog maps

Fig. 4.5: The Defogging Effect Data of Each Algorithm on Two Sets of Real Scene Fog Images

DCP increased the SNR by about 9.5%, the average gradient by about 10.4%, the structural similarity by about 12%, and the information entropy by about 5.8%, indicating that the performance of the algorithm was stable and the IDF effect was good.

4.3. Effect Verification of Landscape IDF System Optimized Based on DCP Algorithm. Combined with the real fog environment, the experiment verified the landscape IDF system optimized based on DCP algorithm. The experimenters input the real landscape fog map into the defogging system and input objective parameters according to the actual situation. The system used Python 3.7 programming language and PyTorch 1.7.1 programming framework, and adopted CUDA 10.1 universal parallel computing architecture. When building a development environment group based on Python+Qt designer, the defogging algorithm was implemented and objective performance parameters were displayed through an interactive interface. The implementation of this system software was achieved by downloading an integrated Python interpreter and

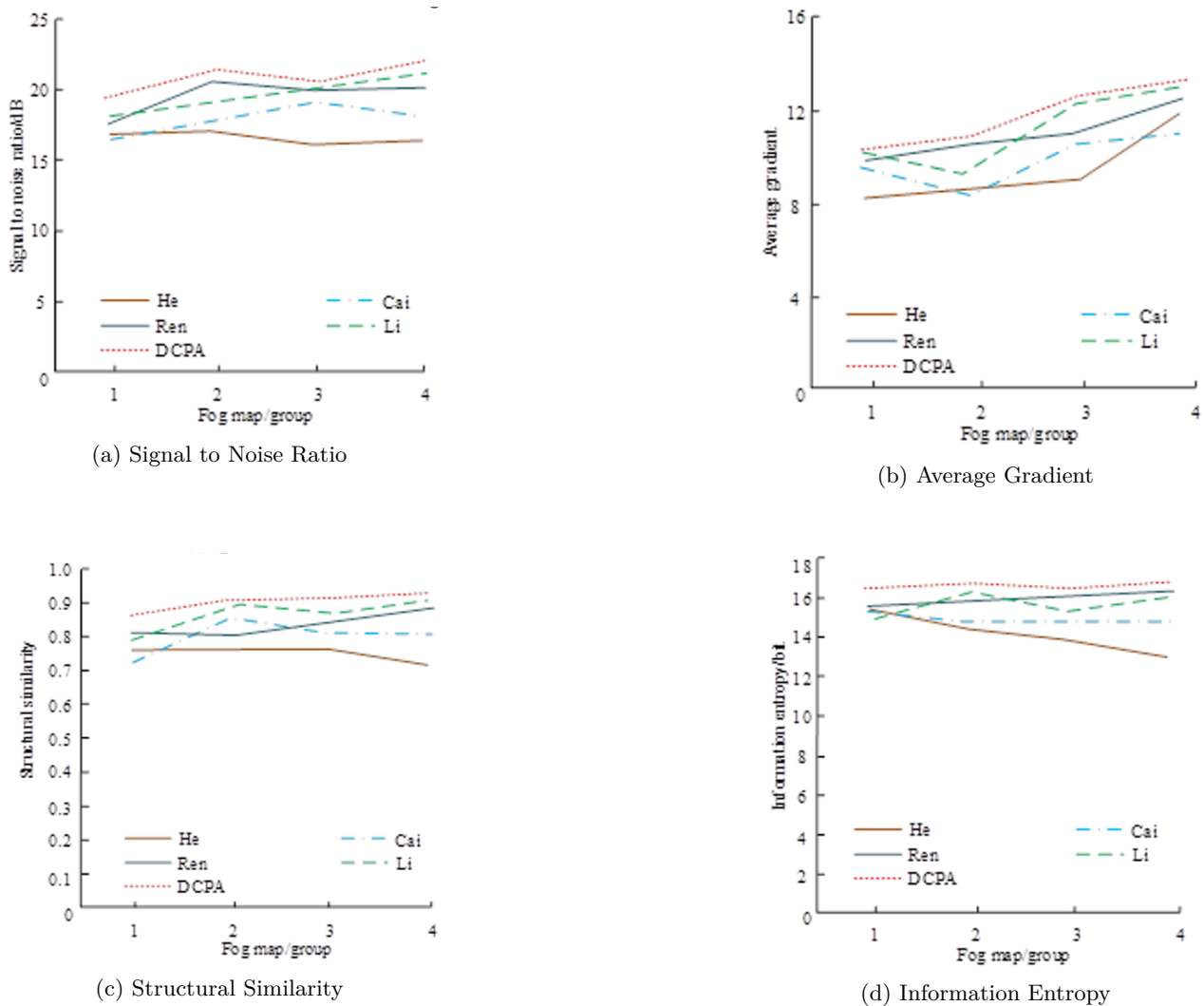


Fig. 4.6: The Defogging Effect Data of Each Algorithm on Two Sets of Real Scene Fog Images

PyQtter integration package based on the VScode editor, and installing PyQt5.0 using a pip pipeline. Real landscape fog maps could be divided into natural, architectural and historical landscapes. The test effect data of landscape IDF system optimized based on DCP algorithm are displayed in Table 4.3.

In Table 4.3 that the SNR and average gradient index were better than logarithmic transform adaptive defogging algorithm, indicating that it had less distortion and higher contrast when the sky area of the image was small. The DCNN defogging algorithm had better structural similarity and information entropy index, indicating that the images processed by it could contain more details, have clear hierarchy and better visual effect, and the fog images with fewer sky areas had better processing effect. In terms of running time, the logarithmic adaptive defogging algorithm had a complex structure, so the running time was longer, which reduced the efficiency of the algorithm. The DCNN algorithm had a less running time, which reduced the complexity of the defogging structure, by contrast, the running time was reduced by about 67%. The results showed that the logarithmic transformation adaptive defogging algorithm had good processing effects in natural landscapes, architectural landscapes, and historical landscapes, with good SNR and average gradient indicators,

Table 4.3: Test Effect Data of the Defogging System

Realistic landscape fog map	Defogging algorithm	SNR/dB	Average gradient	Structural similarity	Information entropy/bit	Run time/s
Natural landscape	Logarithmic transformation adaptation	17.8	10.4	0.8	12.2	7.1
	DCNN	15.6	8.2	0.9	14.9	2.8
Architectural landscape	Logarithmic transformation adaptation	20.3	12.4	0.8	11.8	14.8
	DCNN	17.6	10.7	0.9	15.6	4.1
Historical landscape	Logarithmic transformation adaptation	18.8	10.9	0.8	12.5	7.9
	DCNN	16.8	9.2	0.9	15.9	2.9

as well as high structural similarity and information entropy indicators, resulting in better visual effects. The DCNN defogging algorithm performed better in processing architectural and historical landscapes, with higher structural similarity and information entropy indicators, and performed better in processing fog images with fewer sky areas. In addition, the DCNN defogging algorithm had a shorter running time, which reduced the complexity of the defogging structure and was more suitable for real-time application scenarios. To further verify the use effect of the landscape IDF system optimized based on DCP algorithm, the operability, stability and defogging effect of the system were evaluated in combination with user ratings. Users contain three categories: the first was 10 artists, the second category was 10 defogging system designers, and the third category was 10 random system users. The operability evaluation was a maximum of 10 points, with higher scores indicating better performance. The stability evaluation had a maximum score of 10 points, and the higher the score, the better. The evaluation of defogging effect was a maximum of 10 points, and the higher the score, the better. The user rating results of the landscape IDF system optimized based on the DCP algorithm are shown in Figure 4.7.

Figure 4.7a is the operability score of the system marked by three types of users. In the case of natural landscape fog map processing, the average scores of the three types of users were 9.92 points, 9.89 points and 9.89 points, respectively. In the case of architectural landscape fog map processing, the average scores of the three types of users were 9.85 points, 9.78 points and 9.86 points, respectively. In the case of historical landscape fog map processing, the average scores of the three types of users were 9.91, 9.84 and 9.86 points, respectively. Figure 4.7b shows the three types of users scoring the stability of the system. In natural landscape fog map processing, the average scores of the three types of users were 9.91 points, 9.83 points and 9.89 points, respectively. In architectural landscape fog map processing, the average scores of the three types of users were 9.89 points, 9.79 points and 9.76 points, respectively. In historical landscape fog map processing, the average scores of the three types of users were 9.89 points, 9.79 points and 9.76 points, respectively. The average scores of the three types of users were 9.98, 9.78 and 9.79 points, respectively. Figure 4.7c shows the three types of users scoring the defogging effect of the system. In natural landscape fog map processing, the average scores of the three types of users were 9.71 points, 9.52 points and 9.75 points, respectively. In architectural landscape fog map processing, the average scores of the three types of users were 9.41 points, 9.18 points and 9.22 points, respectively. In historical landscape fog map processing, the average scores of the three types of users were 9.41 points, 9.18 points and 9.22 points, respectively. The average scores of the three types of users were 9.71, 9.49 and 9.86 points, respectively. By analyzing the experimental data, the average scores of operability, stability and defogging effect of the system were 9.87, 9.85 and 9.54 points, respectively. According to the experimental results, different categories of users gave different evaluations of the operability, stability, and defogging effect of the landscape IDF system optimized based on the DCP algorithm. However, considering the average scores of the three types of users, the average scores of the system were all above 9, indicating good performance and good user experience. In addition, the processing effect of the system on fog images varied under different algorithms, but the results all showed good defogging effects.

5. Conclusion. IDF is one of the important image processing techniques, and its application value is high. To raise the effect of landscape IDF, a landscape IDF system based on DCP algorithm was proposed.

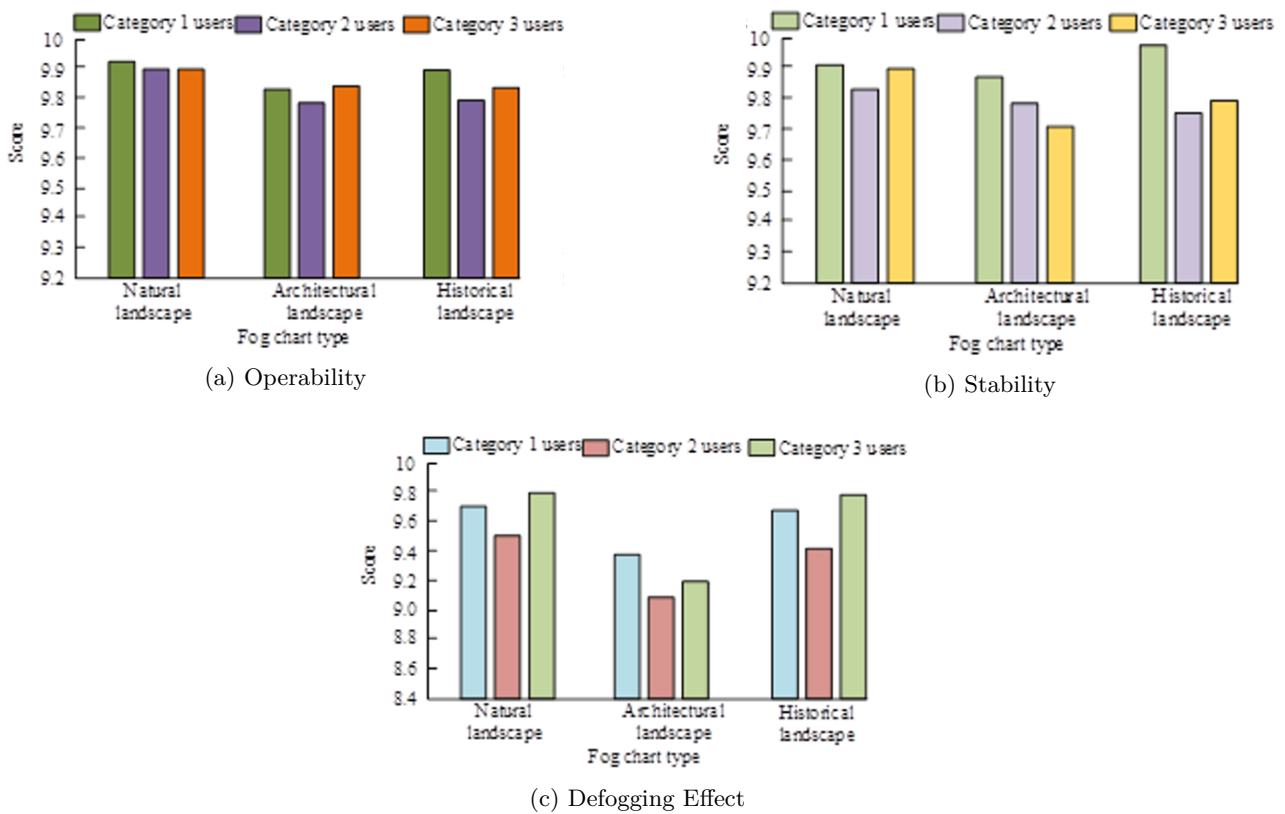


Fig. 4.7: User Rating Results of The Defogging System

Fog image processing was realized by combining the IDF algorithm estimated by AS model and the algorithm based on DCP, and the system design was realized by using the extension package in VS code editor. The experimental data showed that the IDF algorithm estimated by the AS model had the highest SNR, up to 19dB, which was about 15.4% higher than other algorithms on average, indicating that the image was clearer after defogging by this algorithm. The SNR, structural similarity and information entropy of the DCP-based IDF algorithm were above 20, above 0.9 and above 15, indicating that the effect of the DCP-based algorithm was better, and the distortion of the IDF was smaller and clearer. The SNR, average gradient, structural similarity and information entropy of the DCP-based IDF algorithm were increased by about 9.5%, 10.4%, 12% and 5.8%, respectively, indicating that the effectiveness of the algorithm was stable and the IDF effect was good. The DCNN IDF algorithm had less running time and reduced the complexity of the defogging structure, by contrast, it reduced the running time by about 67%. The average score of the system was above 9 points, indicating that the system had good operability, stability, defogging effect, and good user experience. In summary, the IDF system based on the DCP algorithm optimized for landscape images has been verified by experiments. The system performed well in terms of image quality, and its performance could meet the requirements of real-world applications. The DCP algorithm has been proven to be effective in removing fog from the images, and its performance outperformed other state-of-the-art defogging algorithms. The system can handle various types of real-world images, including natural, built-up, and historical landscapes, with good results. The system's high performance is due to the combination of multi-scale parallel feature layers, residual networks, and deep feature fusion. The system's fast performance also contributes to its ability to handle large-scale images. Moreover, the system is user-friendly and has good stability. The IDF algorithm based on DCP can be applied in fields such as photography, computer vision, and remote sensing, helping to improve image quality, fog detection

and semantic segmentation, enhance image super-resolution, and provide an efficient image processing solution. The limitation of this study is that the algorithm performs defogging on degraded images affected by fog during the day. However, when dealing with degraded images such as hail, rainy and snowy weather, and nighttime fog images, the proposed algorithm is not entirely applicable. Future research will focus on studying these different degraded images separately to further enhance the applicability of image processing algorithms.

REFERENCES

- [1] Sharma, N., Kumar, V. & Singla, S. Single image defogging using deep learning techniques: past, present and future. *Archives Of Computational Methods In Engineering*. **28**, 9541-6 (2021,2)
- [2] Zhou, J., Zhang, D. & Zhang, W. Classical and state-of-the-art approaches for underwater image defogging: a comprehensive survey. *Frontiers Of Information Technology & Electronic Engineering*. **21**, 1745-1769 (2020,12)
- [3] Agrawal, S. & Jalal, A. A comprehensive review on analysis and implementation of recent image dehazing methods. *Archives Of Computational Methods In Engineerin..* **29**, 9755-2 (0,5)
- [4] Meng, J., Li, Y., Liang, H. & Ma, Y. Single-image dehazing based on two-stream convolutional neural network. *Journal Of Artificial Intelligence And Technology*. **2**, 100-110 (2022,6)
- [5] Xie, J., Hong, G., Wang, G. & Pen, Z. A variational framework for underwater image dehazing and deblurring. *IEEE Transactions On Circuits And Systems For Video Technology*. **32**, 3514-3526 (2021)
- [6] Sun, Z., Zhang, Y., Bao, F., Wang, P., Yao, X. & Zhang, C. Sadnet: Semi-supervised single image dehazing method based on an attention mechanism. *ACM Transactions On Multimedia Computing, Communications, And Applications (TOMM)..* **18**, 1-23 (2022,2)
- [7] Fan, D., Lu, X., Liu, X., Chi, W. & Liu, S. An iterative defogging algorithm based on pixel-level atmospheric light map. *International Journal Of Modelling, Identification And Control*. **35**, 287-297 (2020)
- [8] Zhao, B. Plateau environment and urban planning based on image defogging algorithm. *Arabian Journal Of Geosciences..* **14**, 1472-1485 (2021,7)
- [9] Long, L., Fu, Y. & Xiao, L. Tropical coastal climate change based on image defogging algorithm and swimming rehabilitation training. *Arabian Journal Of Geosciences..* **14**, 1806-1821 (2021,7)
- [10] He, S., Chen, Z., Wang, F. & Wang, M. Integrated image defogging network based on improved atmospheric scattering model and attention feature fusion, "Earth Science Informatics., vol. 14, no. 4, pp. 2037-2048, Dec. 2021. (0)
- [11] Sun, X., Han, Y., Chen, Y. & Y. Duan, Y. and B. Su, "Aerial Image Defogging Method Based On Nonlocal Feature Structure Tensor By UAV Cameras With Three-channel RGB Cameras," *Journal Of Applied Remote Sensing*. **16**, 46515-46531 (2022,10)
- [12] Hashim, A., Daway, H. & Kareem, H. Single image dehazing by dark channel prior and luminance adjustment. *The Imaging Science Journal*. **68**, 278-287 (2020,3)
- [13] Sun, F., Wang, S., Zhao, G. & Chen, M. Single-image dehazing based on dark channel prior and fast weighted guided filtering. *Journal Of Electronic Imaging*. **30**, 21005-21020 (2021,3)
- [14] Ke, K., Zhang, C., Wu, M. & Sun, Y. Improved defogging algorithm for sea surface images based on dark channel prior theory. *Optical Engineering*. **60**, 21005-21020 (2021,3)
- [15] Yu, X., Xie, W. & Yu, J. Improved defogging algorithm for sea surface images based on dark channel prior theory. *Optical Engineering*. **32**, 441-454 (2022,10)
- [16] Kwak, D. and J. K. Ryu, "A Study On The Dynamic Image-based Dark Channel Prior And Smoke Detection Using Deep Learning," *Journal Of Electrical Engineering & Technology*. **17**, 880-9 (2022,1)
- [17] An, S., Huang, X., Wang, L. & Zheng, Z. Semi-Supervised image dehazing network. *The Visual Computer*. **38**, 202 (0)
- [18] Hassan, H., Bashir, A., Ahmad, M., Menon, V., Afridi, I., Nawaz, R. & Luo, B. Real-time image dehazing by superpixels segmentation and guidance filter. *Journal Of Real-Time Image Processing*. **18**, 202 (0)
- [19] Yao, L. & Pan, Z. The Retinex-based image dehazing using a particle swarm optimization method. *Multimedia Tools And Applications*. **80**, 3425-3442 (2021,1)
- [20] Murthy, N. & Jainuddin, S. An improved dark channel prior based defogging algorithm for video sequences. *Journal Of Information And Optimization Sciences*. **42**, 29-39 (2021,1)
- [21] Guo, Y., Mustafaoglu, Z. & Koundal, D. Spam Detection Using Bidirectional Transformers and Machine Learning Classifier Algorithms. *Journal Of Computational And Cognitive Engineering*. **2**, 5-9 (2022,4)
- [22] Tan, C., Zhao, H. & Ding, H. Statistical initialization of intrinsic K-means clustering on homogeneous manifolds. *Applied Intelligence*. **53**, 3698-8 (2022,6)
- [23] Liu, J., Wang, S., Wang, X., Ju, M. & Zhang, D. A review of remote sensing image dehazing. *Sensors*. **21**, 3926-3948 (2021,6)
- [24] Hu, Q., Zhang, Y., Zhu, Y., Jiang, Y. & Song, M. Single image dehazing algorithm based on sky segmentation and optimal transmission maps. *The Visual Computer*. **39**, 2380-3 (2023,1)
- [25] Yang, G. & Evans, A. Improved single image dehazing methods for resource-constrained platforms. *Journal Of Real-Time Image Processing*. **18**, 1143-6 (2021,12)
- [26] Deeba, F., Dharejo, F., Zawish, M., Memon, F., Dev, K., Naqvi, R. & Du, Y. A novel image dehazing framework for robust vision-based intelligent systems. *International Journal Of Intelligent Systems*. **37**, 10495-10513 (2022,8)
- [27] Ramisetty, S., Anand, D., Kavita, Verma, S., Jhanjhi, N. & Humayun, M. Energy-efficient model for recovery from multiple cluster nodes failure using moth flame optimization in wireless sensor networks. *Intelligent Computing And Innovation On Data Science: Proceedings Of ICTIDS 2021*. pp. 491-499 (2021)

- [28] Humayun, M., Jhanjhi, N., Alruwaili, M., Amalathas, S., Balasubramanian, V. & Selvaraj, B. Privacy protection and energy optimization for 5G-aided industrial Internet of Things. *IEEE Access*. **8** pp. 183665-183677 (2020)
- [29] Lim, M., Abdullah, A. & Jhanjhi, N. Performance optimization of criminal network hidden link prediction model with deep reinforcement learning. *Journal Of King Saud University-Computer And Information Sciences*. **33**, 1202-1210 (2021)

Edited by: Zhengyi Chai

Special issue on: Data-Driven Optimization Algorithms for Sustainable and Smart City

Received: Dec 4, 2023

Accepted: Feb 1, 2024